ARL-TR-85-9



# COMPUTER SIMULATION OF THE EFFECTS OF A DISTRIBUTED ARRAY ANTENNA ON SYNTHETIC APERTURE RADAR IMAGES

FINAL REPORT UNDER CONTRACT NAS9-17228

James M. Estes

APPLIED RESEARCH LABORATORIES
THE UNIVERSITY OF TEXAS AT AUSTIN
POST OFFICE BOX 8029, AUSTIN, TEXAS 78713-8029

9 April 1985

Final Report

1 September 1984 – 15 March 1985

Approved for public release;
distribution unlimited.

*Prepared for:*

NATIONAL AERONAUTICS AND SPACE ADMINISTRATION
LYNDON B. JOHNSON SPACE CENTER
HOUSTON, TX 77058



UNCLASSIFIED

SECURITY CLASSIFICATION OF THIS PAGE (When Data Entered)

| REPORT DOCUMENTATION PAGE | | READ INSTRUCTIONS BEFORE COMPLETING FORM |
|---|---|---|
| 1. REPORT NUMBER | 2. GOVT ACCESSION NO. | 3. RECIPIENT'S CATALOG NUMBER |
| 4. TITLE (and Subtitle)<br>COMPUTER SIMULATION OF THE EFFECTS OF A DISTRIBUTED ARRAY ANTENNA ON SYNTHETIC APERTURE RADAR IMAGES<br>Final Report under Contract NAS9-17228 | | 5. TYPE OF REPORT & PERIOD COVERED<br>final report<br>1 Sep 84 - 15 Mar 85<br>6. PERFORMING ORG. REPORT NUMBER<br>ARL-TR-85-9 |
| 7. AUTHOR(s)<br>James M. Estes | | 8. CONTRACT OR GRANT NUMBER(s)<br>NAS9-17228 |
| 9. PERFORMING ORGANIZATION NAME AND ADDRESS<br>Applied Research Laboratories<br>The University of Texas at Austin<br>Austin, TX 78713-8029 | | 10. PROGRAM ELEMENT, PROJECT, TASK AREA & WORK UNIT NUMBERS |
| 11. CONTROLLING OFFICE NAME AND ADDRESS<br>National Aeronautics and Space Administration<br>Lyndon B. Johnson Space Center<br>Houston, Texas 77058 | | 12. REPORT DATE<br>9 April 1985<br>13. NUMBER OF PAGES<br>27 |
| 14. MONITORING AGENCY NAME & ADDRESS(if different from Controlling Office) | | 15. SECURITY CLASS. (of this report)<br>UNCLASSIFIED<br>15a. DECLASSIFICATION/DOWNGRADING SCHEDULE |

16. DISTRIBUTION STATEMENT (of this Report)

Approved for public release; distribution unlimited.

17. DISTRIBUTION STATEMENT (of the abstract entered in Block 20, if different from Report)

18. SUPPLEMENTARY NOTES

19. KEY WORDS (Continue on reverse side if necessary and identify by block number)

synthetic aperture radar
orbital SAR
simulation
SAR image analysis

20. ABSTRACT (Continue on reverse side if necessary and identify by block number)

The ARL:UT orbital SAR simulation has been upgraded to use three-dimensional antenna gain patterns. This report describes the modifications and presents quantitative image analyses of a simulation using antenna patterns generated from the modeling of a distributed array antenna.

DD FORM 1 JAN 73 1473 EDITION OF 1 NOV 65 IS OBSOLETE

UNCLASSIFIED

SECURITY CLASSIFICATION OF THIS PAGE (When Data Entered)

TABLE OF CONTENTS

LIST OF FIGURES

LIST OF TABLES

# I. INTRODUCTION

## A. Background

Under National Aeronautics and Space Administration Contracts NAS9-15401 and NAS9-15217, Subtask 1, Applied Research Laboratories, The University of Texas at Austin (ARL:UT), developed a computer model of an orbiting synthetic aperture radar (SAR). This model enables the user to create a terrain model of point reflectors on an arbitrarily specifiable planet. The antenna is modeled by its gain pattern in azimuth and elevation and is fixed to the orbiter in accordance with the platform attitude and rates of change of attitude. The transmitter and receiver are specified by frequency, pulse repetition rate (PRF), impulse response characteristics, sampling rate, and range pulse compression codes. Orbital conditions are specified, as well as the area on the planet to be mapped and the geometry of the radar with respect to the area to be mapped. Synthetic in-phase and quadrature (IPQ) video data are then produced as the convolution of received scatterer echoes with the transmitted waveform. The effects of antenna illumination, $R^4$ attenuation, ambiguous ranging, and Doppler sampling are all taken into account. The IPQ video data are then processed through an SAR processor, and the resulting digital images are available for display and analysis. While the scope of the model is limited in some respects, it provides a powerful tool for certain parametric analyses (e.g., the effects of a parameter or part of an SAR may be investigated in an ideal system).

The computer model developed and documented[1] under the aforementioned contracts is known as the orbital SAR simulation (OSS). Currently, the OSS consists of approximately fifty subroutines and programs and over 4500 lines of code written in FORTRAN IV and implemented on the ARL:UT CYBER 180/830. Since the completion of the OSS

version documented in Ref. 1, the OSS has been adapted to two subsequent tasks.[2,3]

## B. Distributed SAR Simulation

This report under NAS9-17228 describes the effort to assess the effects of degradation in a distributed array antenna on SAR images. This study was performed in conjunction with the Physical Science Laboratory, New Mexico State University (PSL/NMSU). PSL/NMSU studied the effects of manufacturing tolerances of a distributed array antenna on its gain pattern. Amplitude and phase variations in the transmit/receive module were considered as were mechanical deformations. Then PSL/NMSU generated computer compatible tapes with three-dimensional gain patterns from arrays with various levels of degradations.

The OSS was modified to use the antenna patterns generated by PSL/NMSU. A series of simulations representative of the shuttle imaging radar (SIR-C) were then executed. The antenna studies and the simulations were performed at C-band, 5.3 GHz. Two computer compatible tapes containing five antenna patterns each were received from PSL/NMSU; a summary of the data received is presented in Table I. The approach taken in this study was to set up a simulation and execute it using the ideal antenna pattern (tape DSAR2, file 1). The same simulation was then run with degraded antenna patterns and the resulting images were compared.

In previous SAR studies ARL:UT adopted a set of "image quality" parameters to characterize an SAR image.[4] Most of these parameters (i.e., resolution, geometric fidelity, crispness, speckle, etc.) are a function of orbit geometry, radar hardware, or SAR processing parameters, and they would not be affected by variations in the antenna gain patterns. However, the extraction of backscatter levels ($\sigma^o$) from the terrain is very likely to be affected by degradations in the antenna gain patterns. By placing fields with known values of $\sigma^o$ in the terrain and

TABLE I
PSL/NMSU GENERATED ANTENNA PATTERNS

Data Files on Tape DSAR1

| Data File No. | Description | Gain (dB) |
|---|---|---|
| 1 | 48 x 12 Array 22 dB Taylor elevation Taper - ideal case | 35.29 |
| 2 | 48 x 12 Array 22 dB Taylor elevation Taper - parabolic bow only 0.024 cm | 35.29 |
| 3 | 48 x 12 Array 22 dB Taylor elevation Taper - random T/R module variations at the element level Amplifier variations +1.76 dB , -3.0 dB Phase Variations +/- 10 | 34.84 |
| 4 | 48 x 12 Array 22 dB Taylor elevation Taper - random T/R module variations (T/R module drives entire row) Amplifier variations +1.76 dB , -3.0 dB Phase Amplifier +/- 10 | 35.11 |
| 5 | 48 x 12 Array 22 dB Taylor elevation Taper - parabolic bow (0.024 cm) and random T/R module variations at the element level Amplifier variations +1.76 dB, -3.0 dB Phase variations +/- 10 | 34.81 |

Data Files on Tape DSAR2

288 x 12 Element DSAR Array
22 dB Taylor Elevation Taper
Array dimensions 12.4 x 0.54 m

| Data File No. | Description | Gain (dB) |
|---|---|---|
| 1 | Ideal case - no mechanical deformations No T/R module degradations | 43.98 |
| 2 | Bow only - 0.175 cm parabolic bow No T/R module degradations | 43.96 |
| 3 | Weight only - no mechanical deformations T/R module variations: amplitude +1.76, -3 dB, phase +/- 10 288 x 12 T/R modules (at element level) | 43.63 |
| 4 | Both - 0.175 cm parabolic bow T/R module variations: amplitude +1.76, -3 dB, phase +/- 10 288 x 12 T/R modules (at element level) | 43.59 |
| 5 | Both 2 - 0.175 cm parabolic bow T/R module variations: amplitude +1.76, -3 dB, phase +/- 10 16 x 12 T/R modules (each module feeds a row, in a sub-panel, 18 elements long) | 43.53 |

then extracting the values for $\sigma^0$ from the images, the effects of the antenna degradations on the measurement of $\sigma^0$ can be assessed. It is important at this point to note that the shape of the antenna gain pattern affects the measurement of $\sigma^0$ within an image as a function of both range and azimuth. If the exact pattern is known, however, then the values for $\sigma^0$ may be properly adjusted (assuming there is no asymmetrical structure). We are concerned here with the degradations which cause the antenna pattern to deviate from what was assumed. In other words, we are interested in the effects on an SAR image due to the antenna degradations after the pattern has been measured.

## II. IMPLEMENTATION

### A. OSS Modifications

The basic change required to the OSS was a modification of the program which uses the antenna pattern (program ECHO). The original simulation used elevation and azimuth principal plane cuts to model the antenna. Program ECHO and subroutine ANTWT were modified to use the three-dimensional antenna patterns generated by PSL/NMSU (redesignated PECHO and PANTWT). The antenna patterns were comprised of 181 conical cuts (361 samples per cut, $1^{o}$ in $\phi$ per sample) of $0.5^{o}$ or $0.25^{o}$ in $\theta$ per cut. Since the 3 dB beamwidth in azimuth of the full array was on the order of $0.25^{o}$, an interpolation scheme was also included in program PECHO. For efficiency, the original version of the OSS did not use an interpolation scheme; instead the desired antenna pattern was sufficiently sampled so that interpolation was not necessary. However, in the present case, sufficient sampling of the antenna pattern would have generated more data than could fit into memory. A quadratic fit through three points was used for interpolation.

A program (ANTPSL) was also written to generate the file for use by program PECHO. ANTPSL takes the antenna patterns generated by PSL/NMSU on 9-track computer compatible tapes and decodes them into a binary file. More operator interaction is required in the modified antenna simulation than in the original model, however, because the modified antenna simulation was not fully integrated into the OSS.

### B. Image Analysis

The current version of the OSS provides no software for the extraction of image statistics needed for image quality analyses. The only post-processing routines available (POST) generated a tape for off-line image display on an ARL:UT graphics system, which is no longer

available. A version of program POST (PPOST) was generated which creates a computer tape of the output SAR image for use on an HP 21MX minicomputer with a Grinnel color graphics display (we used only gray scale and an attached Tektronix hard copy unit).

Another version of program POST (PPOSTST) was created which generates a binary file of the SAR image. The structure of the file is compatible with that generated by an SAR processor which uses real radar data.[5] Programs were available from previous work[6] which allowed extraction of statistics (max, min, mean, and standard deviation) from the SAR images. For this study, these programs were used to print the SAR image pixel values from which the locations of the fields in the images could be deduced. Next, the portions of the images containing the fields were statistically analyzed, and normalized cross-section measurements were obtained.

## C. Current Simulation Model

For the simulations performed, the planet modeled was earth. The orbit parameters were chosen to correspond as closely as possible with the shuttle's, 250 km altitude, near-polar orbit. The frequency was C-band (5.3 GHz), the ground range resolution was 25 m with a sample ratio of 2 (i.e., sample interval 1/2 of resolution), and the overlay ratio was 2 (two "looks"). Two simulations were performed at a $20^{o}$ nadir angle and one at a $60^{o}$ nadir angle.

The area of the terrain model to be imaged is shown in Fig. 1. For the $20^{o}$ nadir angle simulation (using the full array) the ambiguity locations were computed (see p. 4/60 of Ref. 1 for a discussion of ambiguity calculations); fields were then placed at these locations so that the ambiguities would be introduced into the images. The antenna pattern and SAR parameters act to suppress these ambiguities. The complete terrain model, used for all three simulations, is shown in Fig. 2. The ambiguity locations for the $60^{o}$ nadir angle simulation are

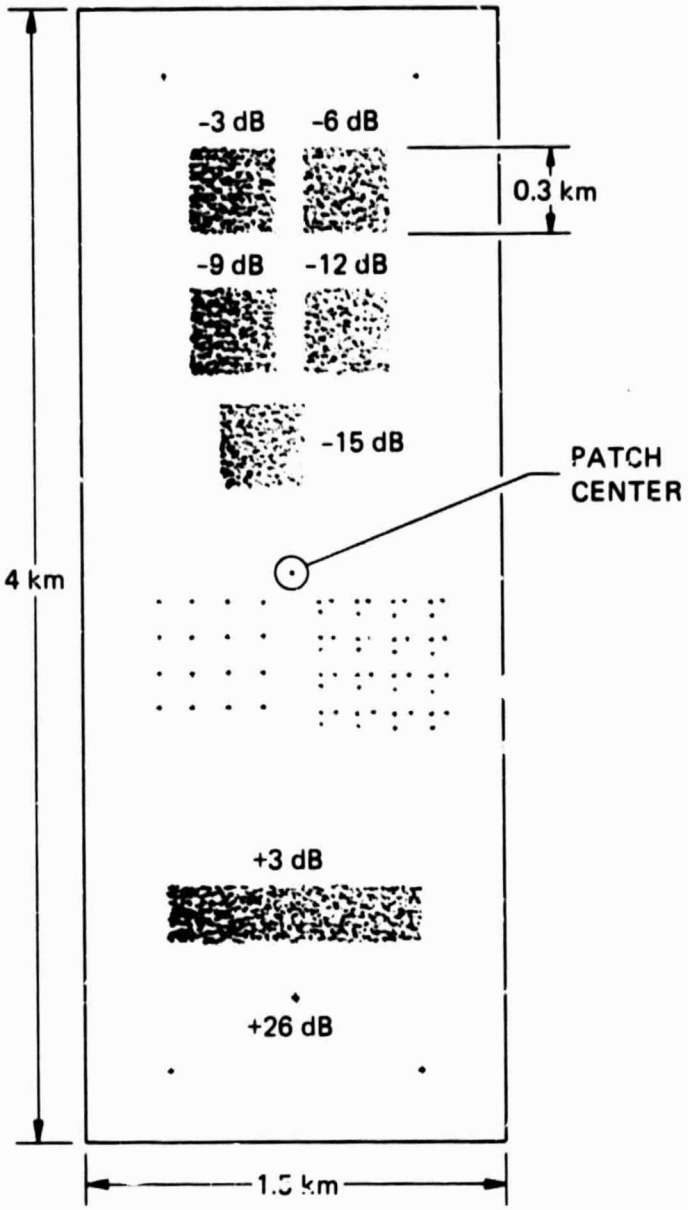


**FIGURE 1**
**AREA OF TERRAIN MODEL IMAGED**
ALL FIELDS CONTAIN 4 SCATTERERS PER RESOLUTION CELL
(25 m x 25 m), WHICH ARE RANDOMLY DISTRIBUTED

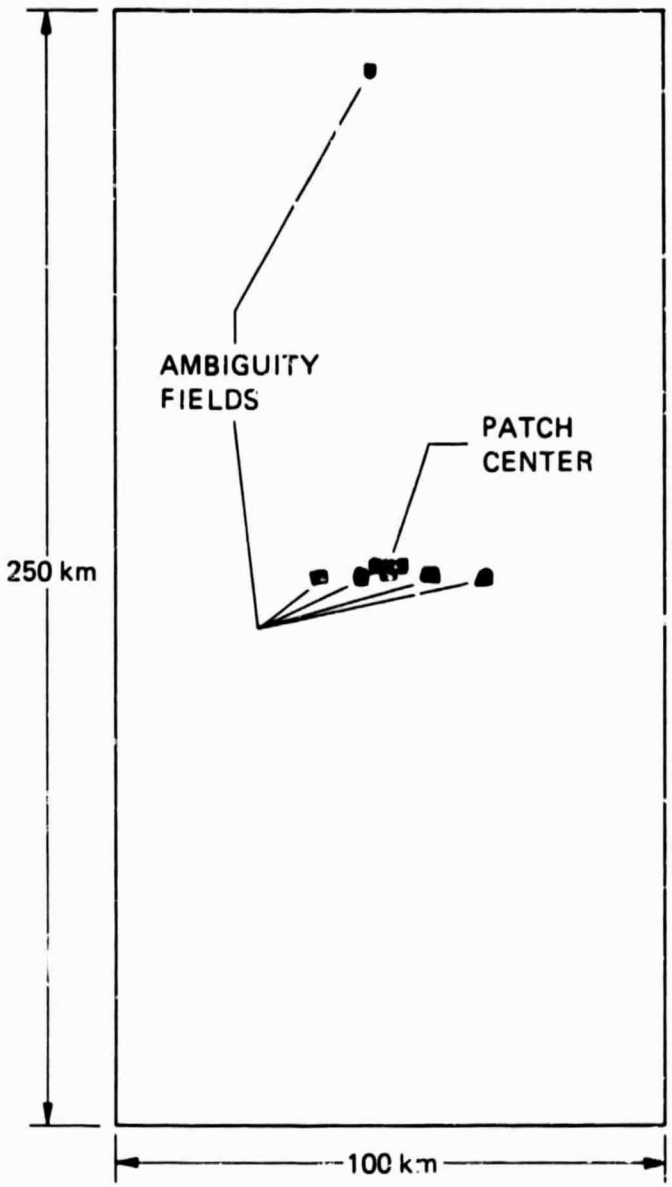


**FIGURE 2**
**COMPLETE TERRAIN MODEL**



ARL:UT
AS-85-408
JME - GA
4 - 10 - 85

different than for the $20^{o}$ nadir angle simulation. However, the unambiguous sector imaged was small, and some of the fields in ambiguity locations fall in the azimuth sidelobes of the antenna pattern. Therefore, the same terrain model could be used for all the simulations.

# III. RESULTS

## A. $60^{o}$ Nadir Angle Simulation

The parameters used for this simulation are shown in Fig. 3. The simulation was exercised for the antenna patterns from tape DSAR2, files 1 and 5 (see Table I). The SAR images produced by the OSS are shown in Fig. 4. The normalized cross-section values from the imaged fields are shown in Table II for the two antenna patterns. Two areas, A1 and A2, are outlined in the SAR images of Fig. 4. These are areas where no targets were placed; the values obtained for A1 and A2 represent ambiguously imaged fields.

The variation in the computed scattering levels for imaged fields within one image is a function of the antenna gain pattern shape and the position of the radar at the start of sampling. The two-way, 3 dB width of the distributed array is approximately $0.2^{o}$; consequently, at a slant range of 530 km, only 1.8 km of the terrain is illuminated. The synthetic array length was 0.7 km. In a real system these variations could be accounted for and need not concern us here. The differences in the values obtained for the ideal and degraded patterns do not take into account the difference in the gain of the two patterns indicated in Table I. For full array patterns (DSAR2) the difference in gain between the two patterns used was 0.45 dB; this translates to a 0.9 dB overall reduction in the degraded pattern results. If a calibration were not performed after deployment of the antenna, this could be significant.

The values obtained for sections A1 and A2 give some idea of the ambiguity level to be expected. It is important to note that the terrain illuminated by the antenna sidelobes was not filled with targets, and therefore the values for A1 and A2 do not represent the integrated sidelobe ratio. However, the fields in the terrain model do fall in the first few major sidelobes, and it is reasonable to expect that the values

```
*********  PLANET SPECIFICATION  *********
PLANET NAME  **                    EARTH                  EQUATORIAL RADIUS (KM)  **            .63781670000E
ECCENTRICITY  **                   .81820179996E-01       GRAVITATIONAL CONSTANT (KM3/SEC2)  ** .39860100000E
ROTATIONAL RATE (DEG/S)  **        .41780745995E-02       TIME OF PRIME MERIDIAN PASSAGE (S) **0.

*********  ORBIT SPECIFICATION  *********
ORBIT I.D.  **                     SHUTTLE                SEMI-MAJOR AXIS (KM)  **              .66780000000E
ECCENTRICITY  **                   .20000000000E-02       INCLINATION (DEG)  **                 .10800000000E
LONG OF ASCENDING NODE (DEG)  **   0.                     ARGUMENT OF PERIGEE (DEG)  **         0.
TIME OF PERIGEE PASSAGE (S)  **    0.                     ROTATIONAL RATE (DEG/S)  **           .67037540870E
ORBITER INITIALIZATION TIME(S)  ** -.10000000000E-03

*********  RADAR SPECIFICATION  *********
RADAR I.D.  **                     SIR-C                  OPERATING WAVELENGTH (M)  **          .56600000000E
RECEIVER/TRANSMITTER BW (MHZ)  **  .66605155813E+01       RANGE TIME-BANDWIDTH PRODUCT  **      .10000000000E
SIGNAL-TO-NOISE RATIO (DB)  **     .10000000000E+03       A/D SAMPLE RATE (MHZ)  **             .13321031163E
SAMPLE LENGTH OF RANGE CORRELATION **              1      SAMPLE LENGTH ACROSS PHASE INTERVAL *
BINARY PHASE CODE  **              B                      BINARY PHASE CODE SEQUENCE  **        RANDOM
GROUND RANGE RESOLUTION (M)  **    .25000000000E+02       AZIMUTH RESOLUTION (M)  **            .25000000000E
RANGE SAMPLING RATIO (M)  **       .20000000000E+01       AZIMUTH SAMPLING RATIO (M)  **        .20000000000E
RANGE IMPULSE RESPONSE FUNCTION  ** COSINE**2             APERTURE WEIGHT FUNCTION  **          TAYLOR
PATCH-TO-PATCH OFFSET, RNG (M)  **  0.                     PATCH-TO-PATCH OFFSET, AZ (M)  **     0.
RANGE SWATH WIDTH (KM)  **         .40000000000E+01       NO OF PATCHES  **
MAP START LATITUDE (DEG)  **       .45000000000E+02

*********  ANTENNA SPECIFICATION  *********
ANTENNA I.D.  **                   6-PANEL-C              BORESIGHT NADIR AT TO (DEG)  **       .60000000000E
BORESIGHT SQUINT AT TO (DEG)  **   .90000000000E+02       AZIMUTH ANGULAR COVERAGE (DEG)  **    .30000000000E
ELEVATION ANGULAR COVERAGE (DEG)  ** .62000000000E+01     PHASE CENTER, BODY AXIS X (M)  **     0.
PHASE CENTER, BODY AXIS Y (M)  **  0.                     PHASE CENTER, BODY AXIS Z (M)  **     0.
COORD SYS, BODY AXIS ROLL, (DEG)  ** 0.                   COORD SYS, BODY AXIS PITCH, (DEG) ** -.30000000000E
COORD SYS, BODY AXIS YAW, (DEG)  **  .90000000000E+02     PLAT ROLL RATE (DEG/S)  **            0.
PLAT PITCH RATE (DEG/S)  **        0.                     PLAT YAW RATE (DEG/S)  **             0.

*********  TERRAIN SPECIFICATION  *********
TERRAIN I.D.  **                   ANT-EVAL               NO OF DISCRETES  **
NO OF FIELDS  **                             13           TOTAL NO OF SCATTERERS  **                    7(
X-AXIS COVERAGE (KM)  **           .31000000000E+02       Y-AXIS COVERAGE (KM)  **              .11500000000E
TERRAIN CENTER, R (KM)  **         .63675192370E+04       TERRAIN CENTER, LAT (DEG)  **         .45000000000E
TERRAIN CENTER, LONG (DEG)  **     .34463288002E+03

******  SYNTHETIC ARRAY PARAMETERS  ******
SYNTHETIC ARRAY NO  **                       1            TRANSMISSION START TIME (S)  **       .68663934355E
ARRAY LENGTH (M)  **               .68480571927E+03       ARRAY INCLINATION (DEG)  **           .82591591160E
ARRAY FORMATION TIME (MS)  **      .88183493374E+02       PLATFORM VELOCITY (KM/S)  **          .77656899503E
NO OF PULSES  **                           138            PRF (HZ)  **                          .15637937780E
NO OF RANGE SAMPLES  **                    319            NO. OF AZIMUTH FILTERS  **                    2
PATCH CENTER RANGE SAMPLE NO.  **          160            SLANT RANGE SWATH WIDTH (KM)  **      .36008266331E
SLANT RANGE RESOLUTION (M)  **     .22505202213E+02       SLANT RANGE SAMPLE INTERVAL (M)  **   .11252601106E
START RANGE (KM)  **               .53475779887E+03       RANGE PATCH CENTER (KM)  **           .53654696245E
SQUINT ANGLE PATCH CENTER (DEG)  ** .90041160378E+02      NADIR ANGLE PATCH CENTER (DEG)  **    .60000586690E
LOS AZIMUTH AT PATCH CENTER (DEG) ** -.11136722416E+03    LOS INCIDENCE AT PATCH CENTER (DEG)** .64185433038E
PATCH CENTER, R (KM)  **           .63675192370E+04       ORBITER MASS CENTER, R (KM)  **       .66188109598E
PATCH CENTER, LAT (DEG)  **        .45000000000E+02       ORBITER MASS CENTER, LAT (DEG)  **    .43347470309E
PATCH CENTER, LONG (DEG)  **       .34463288002E+03       ORBITER MASS CENTER, LONG (DEG)  **   .33927066739E
```

FIGURE 3

SARCON DATA 60° NADIR ANGLE SIMULATION

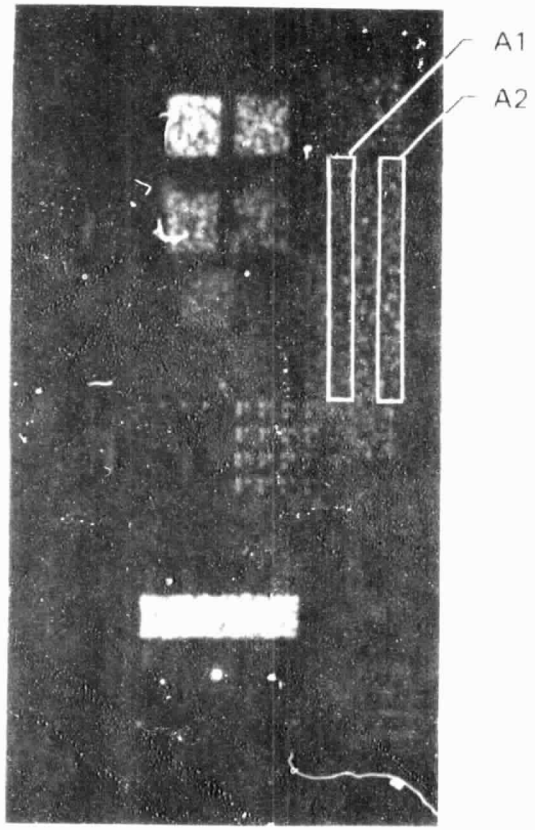


(a) IDEAL PATTERN
DSAR 2, FILE 1

(b) DEGRADED PATTERN
DSAR 2, FILE 5

FIGURE 4
SAR IMAGES FROM 60° NADIR ANGLE SIMULATION

TABLE II

EXTRACTED VALUES FROM SAR IMAGES
FOR THE $60^{o}$ NADIR ANGLE SIMULATION

| FIELD | IDEAL PATTERN DSAR2/File 1 (dB) | DEGRADED PATTERN DSAR2/File 5 (dB) |
|---|---|---|
| - 3 dB | 0.2 | 0.16 |
| - 6 dB | - 4.31 | - 4.35 |
| - 9 dB | - 5.33 | - 5.36 |
| -12 dB | - 9.61 | - 9.61 |
| -15 dB | -11.41 | -11.42 |
| + 3 dB | + 5.96 | + 5.92 |
| A1 | -12.3 | -12.0 |
| A2 | -16.0 | -15.6 |
| Patch Center | - 1.79 | - 1.79 |

for A1 and A2 are within 2-3 dB of the total ambiguity level. From these data we can infer a value for dark target contrast (ratio of the mean level of an area of very low reflectance to the mean level of the entire image) of approximately -14 dB. It appears that most of the energy is from a field ambiguously imaged in the main lobe.

## B. $20^{o}$ Nadir Angle Simulation

The parameters used for this simulation are shown in Fig. 5. The simulation was performed using files 1 and 5 from DSAR2. The SAR images produced are shown in Fig. 6. Table III is a list of the extracted values from the images. As pointed out in Section III.A, the variation in reflectivity level, in azimuth, across the image is due to the shape of the antenna gain pattern.

For this simulation, the values for ambiguous areas A1 and A2 are much lower than in the previous simulation. The pulse repetition frequency (PRF) for this simulation unambiguously images $0.5^{o}$ at the main beam, instead of the $0.3^{o}$ imaged in the previous simulation.

## C. $20^{o}$ Nadir Angle Simulation, Short Array

The geometry of this simulation was identical to the previous $20^{o}$ nadir angle case. The antenna patterns used, however, were from tape DSAR1 (see Table I). These patterns were created from one panel (out of six) of the distributed array antenna and have a corresponding beamwidth six times that of the full array in azimuth (elevation dimensions are identical). To avoid ambiguity problems, a higher PRF was used.

The parameters used for this simulation are shown in Fig. 7. The SAR images produced using the antenna patterns from DSAR1, files 1, 4, and 5, are shown in Fig. 8. The corresponding values for normalized cross-section are presented in Table IV.

```
********* PLANET SPECIFICATION *********
PLANET NAME **                    EARTH                  EQUATORIAL RADIUS (KM) **              .63781670000E
ECCENTRICITY **                   .81820179996E-01       GRAVITATIONAL CONSTANT (KM3/SEC2) **   .39860100000E
ROTATIONAL RATE (DEG/S) **        .41780745995E-02       TIME OF PRIME MERIDIAN PASSAGE (S) **0.

********* ORBIT SPECIFICATION **********
ORBIT I.D. **                     SHUTTLE                SEMI-MAJOR AXIS (KM) **                .66280000000E
ECCENTRICITY **                   .20000000000E-02       INCLINATION (DEG) **                   .10800000000E
LONG OF ASCENDING NODE (DEG) **   0.                     ARGUMENT OF PERIGEE (DEG) **           0.
TIME OF PERIGEE PASSAGE (S) **    0.                     ROTATIONAL RATE (DEG/S) **             .67037540870E
ORBITER INITIALIZATION TIME(S) ** -.10000000000E-03

********* RADAR SPECIFICATION **********
RADAR I.D. **                     SIR-C                  OPERATING WAVELENGTH (M) **            .56600000000E
RECEIVER/TRANSMITTER BW (MHZ) **  .16863430288E+02       RANGE TIME-BANDWIDTH PRODUCT **        .10000000000E
SIGNAL-TO-NOISE RATIO (DB) **     .10000000000E+03       A/D SAMPLE RATE (MHZ) **               .33726860576E
SAMPLE LENGTH OF RANGE CORRELATION **              1     SAMPLE LENGTH ACROSS PHASE INTERVAL *
BINARY PHASE CODE **              B                      BINARY PHASE CODE SEQUENCE **          RANDOM
GROUND RANGE RESOLUTION (M) **    .25000000000E+02       AZIMUTH RESOLUTION (M) **              .25000000000E
RANGE SAMPLING RATIO (M) **       .20000000000E+01       AZIMUTH SAMPLING RATIO (M) **          .20000000000E
RANGE IMPULSE RESPONSE FUNCTION ** COSINE**2             APERTURE WEIGHT FUNCTION **            TAYLOR
PATCH-TO-PATCH OFFSET, RNG (M) ** 0.                     PATCH-TO-PATCH OFFSET, AZ (M) **       0.
RANGE SWATH WIDTH (KM) **         .40000000000E+01       NO OF PATCHES **
MAP START LATITUDE (DEG) **       .45000000000E+02

********* ANTENNA SPECIFICATION **********
ANTENNA I.D. **                   6-PANEL-C              BORESIGHT NADIR AT TO (DEG) **         .20000000000E
BORESIGHT SQUINT AT TO (DEG) **   .90000000000E+02       AZIMUTH ANGULAR COVERAGE (DEG) **      .50000000000E
ELEVATION ANGULAR COVERAGE (DEG) ** .62000000000E+01     PHASE CENTER, BODY AXIS X (M) **       -.34000000000E
PHASE CENTER, BODY AXIS Y (M) **  0.                     PHASE CENTER, BODY AXIS Z (M) **       0.
COORD SYS, BODY AXIS ROLL, (DEG) ** 0.                   COORD SYS, BODY AXIS PITCH, (DEG) **   -.70000000000E
COORD SYS, BODY AXIS YAW, (DEG) ** .90000000000E+02      PLAT ROLL RATE (DEG/S) **              0.
PLAT PITCH RATE (DEG/S) **        0.                     PLAT YAW RATE (DEG/S) **               0.

********* TERRAIN SPECIFICATION **********
TERRAIN I.D. **                   ANT-EVAL               NO OF DISCRETES **
NO OF FIELDS **                                  13      TOTAL NO OF SCATTERERS **                              7
X-AXIS COVERAGE (KM) **           .31000000000E+02       Y-AXIS COVERAGE (KM) **                .11500000000E
TERRAIN CENTER, R (KM) **         .63675192370E+04       TERRAIN CENTER, LAT (DEG) **           .45000000000E
TERRAIN CENTER, LONG (DEG) **     .33937463695E+03

****** SYNTHETIC ARRAY PARAMETERS ******
SYNTHETIC ARRAY NO **                            1       TRANSMISSION START TIME (S) **         .70807617257E
ARRAY LENGTH (M) **               .34254838328E+03       ARRAY INCLINATION (DEG) **             .84558418492E
ARRAY FORMATION TIME (MS) **      .44112102067E+02       PLATFORM VELOCITY (KM/S) **            .77654057315E
NO OF PULSES **                                115       PRF (HZ) **                            .26050123591E
NO OF RANGE SAMPLES **                         319       NO. OF AZIMUTH FILTERS **
PATCH CENTER RANGE SAMPLE NO. **               160       SLANT RANGE SWATH WIDTH (KM) **        .14221775309E
SLANT RANGE RESOLUTION (M) **     .88888350377E+01       SLANT RANGE SAMPLE INTERVAL (M) **     .44444175188E
START RANGE (KM) **               .26767702759E+03       RANGE PATCH CENTER (KM) **             .26938368998E
SQUINT ANGLE PATCH CENTER (DEG) ** .90104737538E+02      NADIR ANGLE PATCH CENTER (DEG) **      .20001321723E
LOS AZIMUTH AT PATCH CENTER (DEG) ** -.11489683437E+03   LOS INCIDENCE AT PATCH CENTER (DEG)**  .20827364886E
PATCH CENTER, R (KM) **           .63675192370E+04       ORBITER MASS CENTER, R (KM) **         .66190535439E
PATCH CENTER, LAT (DEG) **        .45000000000E+02       ORBITER MASS CENTER, LAT (DEG) **      .44647387989E
PATCH CENTER, LONG (DEG) **       .33937463695E+03       ORBITER MASS CENTER, LONG (DEG) **     .33832143834E
```

FIGURE 5

SARCON DATA 20° NADIR ANGLE SIMULATION

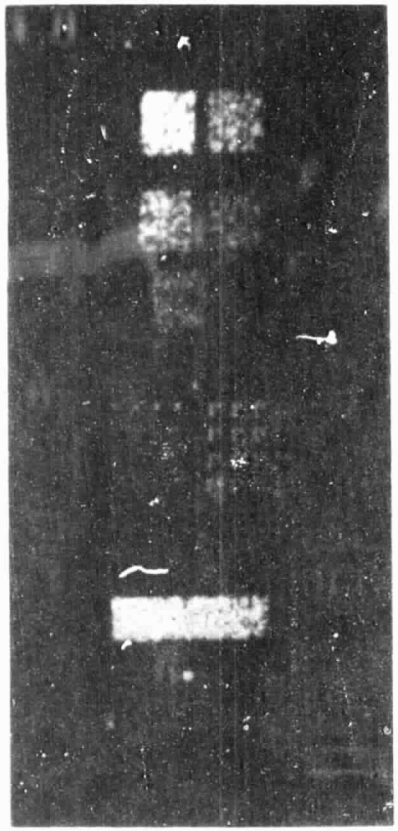

(a) IDEAL PATTERN
DSAR 2, FILE 1

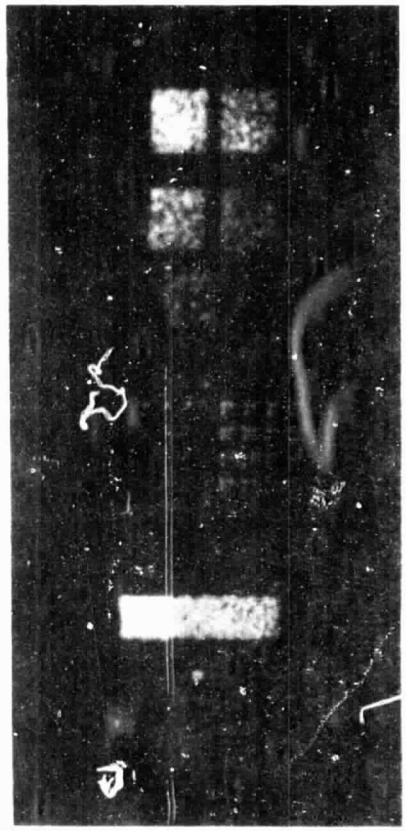

(b) DEGRADED PATTERN
DSAR 2, FILE 5

FIGURE 6
SAR IMAGES FROM 20° NADIR ANGLE SIMULATION

TABLE III

EXTRACTED VALUES FROM SAR IMAGES
FOR THE $20^{o}$ NADIR ANGLE SIMULATION

| FIELD | IDEAL PATTERN DSAR2/File 1 (dB) | DEGRADED PATTERN DSAR2/File 5 (dB) |
|---|---|---|
| - 3 dB | - 0.02 | 0.41 |
| - 6 dB | - 7.13 | - 6.94 |
| - 9 dB | - 5.63 | - 5.96 |
| -12 dB | -12.63 | -12.35 |
| -15 dB | -11.54 | -11.51 |
| + 3 dB | | |
| A1 | -27.6 | -27.8 |
| A2 | -51.8 | -50.7 |
| Patch Center | - 2.02 | - 2.01 |

```
********* PLANET SPECIFICATION *********
NET NAME **                    EARTH                    EQUATORIAL RADIUS (KM) **          .63781670000E+04
ENTRICITY **                   .81820179996E-01         GRAVITATIONAL CONSTANT (KM3/SEC2) **.39860100000E+06
ATIONAL RATE (DEG/S) **        .41780745995E-02         TIME OF PRIME MERIDIAN PASSAGE (S) **0.

********* ORBIT SPECIFICATION *********
IT I.D. **                     SHUTTLE                  SEMI-MAJOR AXIS (KM) **            .66280000000E+04
ENTRICITY **                   .20000000000E-02         INCLINATION (DEG) **               .10800000000E+03
G OF ASCENDING NODE (DEG) **   0.                       ARGUMENT OF PERIGEE (DEG) **       0.
E OF PERIGEE PASSAGE (S) **    0.                       ROTATIONAL RATE (DEG/S) **         .67037540870E-01
ITER INITIALIZATION TIME(S) ** -.10000000000E-03

********* RADAR SPECIFICATION *********
AR I.D. **                     SIR-C                    OPERATING WAVELENGTH (M) **        .56600000000E-01
EIVER/TRANSMITTER BW (MHZ) **  .16863430288E+02         RANGE TIME-BANDWIDTH PRODUCT **    .10000000000E+01
NAL-TO-NOISE RATIO (DB) **     .10000000000E+03         A/D SAMPLE RATE (MHZ) **           .33726860576E+02
IPLE LENGTH OF RANGE CORRELATION **  1                  SAMPLE LENGTH ACROSS PHASE INTERVAL *  1
ARY PHASE CODE **              B                        BINARY PHASE CODE SEQUENCE **      RANDOM
UND RANGE RESOLUTION (M) **    .25000000000E+02         AZIMUTH RESOLUTION (M) **          .25000000000E+02
GE SAMPLING RATIO (M) **       .20000000000E+01         AZIMUTH SAMPLING RATIO (M) **      .20000000000E+01
GE IMPULSE RESPONSE FUNCTION ** COSINE**2               APERTURE WEIGHT FUNCTION **        TAYLOR
CH-TO-PATCH OFFSET, RNG (M) ** 0.                       PATCH-TO-PATCH OFFSET, AZ (M) **   0.
GE SWATH WIDTH (KM) **         .40000000000E+01         NO OF PATCHES **                   2
 START LATITUDE (DEG) **       .45000000000E+02

********* ANTENNA SPECIFICATION *********
ENNA I.D. **                   6-PANEL-C                BORESIGHT NADIR AT TO (DEG) **     .20000000000E+02
ESIGHT SQUINT AT TO (DEG) **   .90000000000E+02         AZIMUTH ANGULAR COVERAGE (DEG) **  .15000000000E+01
VATION ANGULAR COVERAGE (DEG) ** .90000000000E+01       PHASE CENTER, BODY AXIS X (M) **   0.
SE CENTER, BODY AXIS Y (M) **  0.                       PHASE CENTER, BODY AXIS Z (M) **   0.
RD SYS, BODY AXIS ROLL, (DEG) ** 0.                     COORD SYS, BODY AXIS PITCH, (DEG) ** -.70000000000E+02
RD SYS, BODY AXIS YAW, (DEG) ** .90000000000E+02        PLAT ROLL RATE (DEG/S) **          0.
T PITCH RATE (DEG/S) **        0.                       PLAT YAW RATE (DEG/S) **           0.

********* TERRAIN SPECIFICATION *********
RAIN I.D. **                   ANT-EVAL                 NO OF DISCRETES **                 71
 OF FIELDS **                  13                       TOTAL NO OF SCATTERERS **          7095
XIS COVERAGE (KM) **           .31000000000E+02         Y-AXIS COVERAGE (KM) **            .11500000000E+03
RAIN CENTER, R (KM) **         .63675192370E+04         TERRAIN CENTER, LAT (DEG) **       .45000000000E+02
RAIN CENTER, LONG (DEG) **     .33937463695E+03

****** SYNTHETIC ARRAY PARAMETERS ******
THETIC ARRAY NO **             1                        TRANSMISSION START TIME (S) **     .70807617257E+03
AY LENGTH (M) **               .34254838328E+03         ARRAY INCLINATION (DEG) **         .84558418492E-01
AY FORMATION TIME (MS) **      .44112102067E+02         PLATFORM VELOCITY (KM/S) **        .77654057315E+01
 OF PULSES **                  333                      PRF (HZ) **                        .75545358413E+04
 OF RANGE SAMPLES **           319                      NO. OF AZIMUTH FILTERS **          200
CH CENTER RANGE SAMPLE NO. **  160                      SLANT RANGE SWATH WIDTH (KM) **    .14221775309E+01
NT RANGE RESOLUTION (M) **     .88888350377E+01         SLANT RANGE SAMPLE INTERVAL (M) ** .44444175188E+01
RT RANGE (KM) **               .26767702759E+03         RANGE PATCH CENTER (KM) **         .26838368998E+03
JINT ANGLE PATCH CENTER (DEG) ** .90104737538E+02       NADIR ANGLE PATCH CENTER (DEG) **  .20001321723E+02
 AZIMUTH AT PATCH CENTER (DEG) ** -.11489683437E+03     LOS INCIDENCE AT PATCH CENTER (DEG)** .20827364886E+02
CH CENTER, R (KM) **           .63675192370E+04         ORBITER MASS CENTER, R (KM) **     .66190535439E+04
CH CENTER, LAT (DEG) **        .45000000000E+02         ORBITER MASS CENTER, LAT (DEG) **  .44647387989E+02
CH CENTER, LONG (DEG) **       .33937463695E+03         ORBITER MASS CENTER, LONG (DEG) ** .33832143834E+03
```

FIGURE 7

SARCON DATA 20° NADIR ANGLE SIMULATION, SHORT ARRAY

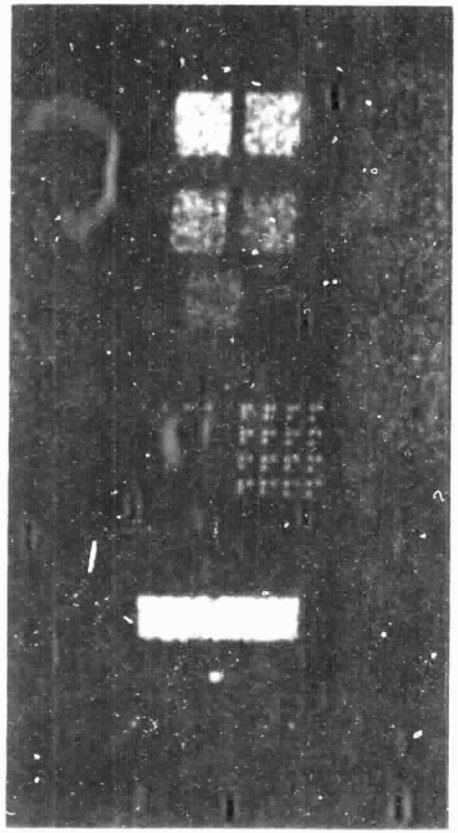

(a) IDEAL PATTERN
DSAR 1, FILE 1

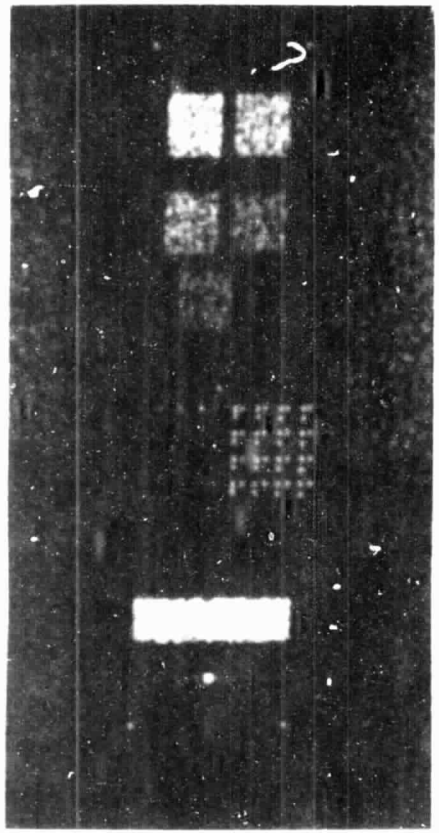

(b) DEGRADED PATTERN
DSAR 1, FILE 4

(c) DEGRADED PATTERN
DSAR1, FILE 5

FIGURE 8
SAR IMAGES FROM 20° NADIR ANGLE SIMULATION, SHORT ARRAY

TABLE IV

EXTRACTED VALUES FROM SAR IMAGES
FOR THE $20^{o}$ NADIR ANGLE SIMULATION, SHORT ARRAY

| FIELD | IDEAL PATTERN DSAR2/File 1 (dB) | DEGRADED PATTERN DSAR1/File 4 (dB) | DEGRADED PATTERN DSAR1/File 5 (dB) |
|---|---|---|---|
| - 3 dB | + 1.64 | + 1.70 | + 1.64 |
| - 6 dB | - 1.68 | - 1.68 | - 1.70 |
| - 9 dB | - 4.88 | - 4.86 | - 4.88 |
| -12 dB | - 7.53 | - 7.52 | - 7.53 |
| -15 dB | - 9.91 | - 9.90 | - 9.91 |
| + 3 dB | | + 7.82 | + 7.87 |
| A1 | -20.4 | -20.4 | -20.4 |
| A2 | -16.8 | -16.8 | -16.8 |
| Patch Center | + 0.05 | + 0.05 | + 0.05 |

# IV. CONCLUSIONS AND RECOMMENDATIONS

The OSS has been modified to use three-dimensional antenna patterns (specified as conical cuts). The simulation analyzed in this report was exercised on three configurations with seven complete simulations. A copy of the OSS modifications and programs used to analyze the images has been sent to NASA/JSC on computer compatible tape, along with another copy of the original OSS.

The results summarized in Tables II-IV show very little effect due to distortions in the shape of the antenna patterns. The effect on the images due to pattern distortions is on the order of a few tenths of a decibel. Additionally there is a reduction in overall gain of up to 0.9 dB for the degraded patterns (see Table I for the one-way gain reductions). A comparison of the antenna patterns received from PSL/NMSU shows virtually no perceptible main beam distortion or pointing error.

The results of this study show that, for the electrical variations in T/R modules on the order of +1.8/-3 dB and $\pm 10^{0}$ phase, the effects on the SAR images are negligible except for a gain factor which would presumably be measured after antenna construction and before deployment. Implicit in the previous statement is the assumption that the electrical variations are the result of manufacturing tolerances and are not time dependent. It is appropriate to note here that the antenna patterns were modeled as gain versus angle, and that if there are any phase distortions with angle across the main beam, then several parameters in an image including resolution and SAR beamforming could be affected. The mechanical deformations which were modeled, however, represent symmetrical variations in the manufacture of the antenna and may not be representative of errors in the deployment of the antenna in space. Asymmetrical mechanical deformations may be more serious than what have been modeled to date.

Effects on the SAR image not fully modeled in this study include the effects of ambiguities. The PRFs proposed for the SIR-C (1200-1900 pulses/s) will not allow unambiguous imaging of the main lobe of the antenna pattern. In the $60^{o}$ nadir simulation performed in this study, the PRF was 1570 Hz, which corresponds to an unambiguous imaging coverage of $0.3^{o}$. The one-way 6 dB width of the main lobe of the full array is approximately $0.3^{o}$, so that for this set-up ambiguous returns on the order of -12 dB would be observed. The other mechanism for ambiguous imaging is the reception of scattered energy in the sidelobes of the antenna. Without shading, the azimuth sidelobes are on the order of -13 dB from the peak. Since ambiguous imaging through azimuth sidelobes occurs from both transmission and reception through the sidelobes, the received energy will be 26 dB below the peak. In the case of range ambiguities which occur by eclipsing of the received pulses, however, energy transmitted on several pulses is received through the range sidelobes of each pulse, thus effectively changing the range sidelobe pattern by up to 10 dB. The range sidelobes of the patterns generated by PSL/NMSU were 22-24 dB below the peak (22 dB Taylor weighting was used). For the single panel case generated by PSL/NMSU, with T/R modules driving rows of 48 elements, the range sidelobes were only 19 dB down from the peak. Depending on the configuration, these may be unacceptably high.

Future studies could take two paths. One would be to more closely model the proposed SIR-C and investigate the effects of ambiguities and mechanical deformations of the antenna. The second line of research would be to investigate the possible effects of mechanical deformations due to deployment, thermal gradients, and other time varying factors on the SAR images. Since measurement of the antenna gain pattern after deployment does not seem possible, these time varying factors can create irrecoverable errors in the SAR images.

## REFERENCES


1. Gary L. Crow and Kermit E. Graf, "Imaging Radar Simulation and Signal Processing Software, Vol. I, An Orbital SAR Simulation Program," Applied Research Laboratories Technical Report No. 79-58 (ARL-TR-79-58), Applied Research Laboratories, The University of Texas at Austin, November 1979.

2. Carroll R. Griffin and James M. Estes, "Mathematical Modeling and SAR Simulation Multifunction Technology Efforts," Applied Research Laboratories Technical Report No. 81-41 (ARL-TR-81-41), Applied Research Laboratories, The University of Texas at Austin, September 1981.

3. James M. Estes, "Computer Modeling of a Wideswath SAR Concept Employing Multiple Antenna Beam Formation Techniques," Applied Research Laboratories Technical Report No. 82-57 (ARL-TR-82-57), Applied Research Laboratories, The University of Texas at Austin, September 1982.

4. F. A. Collins et al., "FLAMR Image Quality Studies and Processing Tradeoff Experiments" (U), Applied Research Laboratories Technical Report No. 75-31 (ARL-TR-75-31), Applied Research Laboratories, The University of Texas at Austin, May 1975. (CONFIDENTIAL)

5. Carroll R. Griffin and James M. Estes, "Development of a Ground Signal Processor for Digital Synthetic Array Radar Data," Applied Research Laboratories Technical Report No. 81-21 (ARL-TR-81-21), Applied Research Laboratories, The University of Texas at Austin, May 1981.

6. Carroll R. Griffin and James M. Estes, "APQ-102 Imaging Radar Digital Image Quality Study," Applied Research Laboratories Technical Report No. 82-68 (ARL-TR-82-68), Applied Research Laboratories, The University of Texas at Austin, November 1982.